The Astrophysical Journal Letters, 880:L9 (7pp), 2019 July 20 https://doi.org/10.3847/2041-8213/ab2f8c

Beyond *UVJ*: More Efficient Selection of Quiescent Galaxies with Ultraviolet/Mid-infrared Fluxes

Joel Leja, Sandro Tacchella, and Charlie Conroy
Harvard-Smithsonian Center for Astrophysics, 60 Garden St. Cambridge, MA 02138, USA; joel.leja@cfa.harvard.edu, sandro.tacchella@cfa.harvard.edu
Received 2019 March 15; revised 2019 June 27; accepted 2019 July 3; published 2019 July 18

Abstract

The *UVJ* color–color diagram is a popular and efficient method to distinguish between quiescent and star-forming galaxies through their rest-frame *U*–*V* versus *V*–*J* colors. Here we explore the information content of this color–color space using the Bayesian inference machine `Prospector`. We fit the same physical model to two data sets: (i) *UVJ* fluxes alone, and (ii) full UV–mid IR (MIR) broadband spectral energy distributions from the 3D-*HST* survey. Notably this model uses both nonparametric star formation histories and a flexible dust attenuation curve, both of which have the potential to "break" the typical correlations observed in *UVJ* color–color space. Instead, these fits confirm observed trends between *UVJ* colors and observed galaxy properties, including specific star formation rate (sSFR), dust attenuation, stellar age, and stellar metallicity. They also demonstrate that *UVJ* colors do not, on their own, constrain stellar age or metallicity; the observed trends in the *UVJ* diagram are instead driven by galaxy scaling relationships and thus will evolve with cosmological time. We also show that *UVJ* colors "saturate" below $\log(\mathrm{sSFR}/\mathrm{yr}^{-1}) \lesssim -10.5$, i.e., changing sSFR no longer produces substantial changes in *UVJ* colors. We show that far-UV and/or MIR fluxes continue to correlate with sSFR down to low sSFRs and can be used in color–color diagrams to efficiently target galaxies with much lower levels of ongoing star formation. We provide selection criteria in these new color–color spaces as a function of desired sample sSFR.

Key words: galaxies: high-redshift – galaxies: star formation

1. Introduction

Quantifying the rate of stellar mass assembly in star-forming and quiescent galaxies over the past ∼13 Gyr is necessary to understand how the present-day galaxy population formed. Such an investigation requires large numbers of both star-forming and quiescent galaxies at early epochs. Separating the two populations can be challenging, with the most direct methods requiring expensive spectroscopic measurements such as D_n4000 (Kauffmann et al. 2003) or Hα equivalent width (Brinchmann et al. 2004).

During the last decade, rest-frame color–color diagrams and in particular the *UVJ* diagram have been very popular for separating these two categories of galaxies, in part because they can be efficiently applied to large photometric samples (e.g., Daddi et al. 2004; Williams et al. 2009; Arnouts et al. 2013). Williams et al. (2009) originally devised the *UVJ* color–color selection, based on the corresponding color–color diagram introduced by Wuyts et al. (2007; see also BzK selection, Daddi et al. 2004). This approach uses near-infrared photometry to solve the long-running problem of distinguishing between galaxies that are optically red due to age and galaxies that are optically red due to dust attenuation (e.g., Strateva et al. 2001; Baldry et al. 2004; Balogh et al. 2004. Since then, *UVJ* selection has been used to sort galaxy samples at all cosmic epochs with great success (e.g., Whitaker et al. 2013; Barro et al. 2014; Straatman et al. 2014; Papovich et al. 2018). The efficacy of this selection has been confirmed, with deep MIR imaging revealing low average sSFRs in *UVJ*-selected quiescent galaxies: $\mathrm{sSFR} \sim 10^{-11.9} \times (1+z)^4\ \mathrm{yr}^{-1}$ (Fumagalli et al. 2014). Simulations have even begun assigning *UVJ* colors to their outputs in order to define quiescence (e.g., Davé et al. 2017; Donnari et al. 2019).

However, advances in statistics, modeling, and reams of new data have provided sophisticated tools to evaluate *UVJ* classification in new detail. Recent studies using spectroscopic information (Belli et al. 2017; Schreiber et al. 2018), spectral energy distribution (SED) fitting (Díaz-García et al. 2017; Fang et al. 2018; Merlin et al. 2018), and combinations of methods (Moresco et al. 2013) find that *UVJ*-quiescent selection includes ∼10%–30% contamination from star-forming galaxies. Furthermore, there exist correlations in the quiescent part of the *UVJ* diagram that permit measurements of ages (Whitaker et al. 2013; Belli et al. 2019), and when *UVJ* colors are combined with stellar mass and redshift, it has been claimed that one can measure metallicities, extinctions, and sSFRs as well (Díaz-García et al. 2017).

Building on these findings, here we use the Bayesian inference machine `Prospector` (Johnson & Leja 2017; Leja et al. 2017) to examine the ability of straightforward *UVJ* color–color cuts to diagnose stellar populations properties. Bayesian inference is the natural tool for this task, as it is designed to deal with complex correlations such as those that exist between galaxy properties and rest-frame colors.

Throughout the paper we use a Chabrier (2003) IMF and a WMAP9 (Hinshaw et al. 2013) cosmology. All parameters are reported as the median of their respective probability distribution and all magnitudes are in the AB system.

2. Data and Models

We use the `Prospector` Bayesian inference machine (Johnson & Leja 2017; Leja et al. 2017) to translate galaxy photometry into parameter posteriors. This approach uses the Flexible Stellar Population Synthesis stellar populations (Conroy et al. 2009) code to construct a physical model and the nested sampler `dynesty` (Speagle 2019) to sample the posterior space.

Within the Prospector framework we construct two closely related physical models, one optimized to fit observed panchromatic galaxy SEDs and one to fit synthetic *UVJ* fluxes.

2.1. Fitting Observed Panchromatic Photometry

To better understand how the properties of observed galaxies correlate with their rest-frame *UVJ* colors, we take the physical parameters derived from Prospector fits to the 3D-*HST* photometric catalogs (Skelton et al. 2014) from Leja et al. (2019b).

These fits use a modified version of the Prospector−α physical model, described in detail in Leja et al. (2019b). In brief, this model includes a seven-bin nonparametric star formation history (SFH) with a prior emphasizing smoothness in SFR(t) (Leja et al. 2019a), a two-component dust model with a flexible attenuation curve (Charlot & Fall 2000), free stellar metallicity with a mass–metallicity prior, and hot dust emission from an active galactic nucleus (Leja et al. 2018). This model also includes dust emission via energy balance and nebular emission self-consistently powered by the stellar fluxes.

The 3D-*HST* catalogs provide observed-frame 0.3–24 μm photometry and redshifts for some 200,000 galaxies. These galaxies are in five well-studied extragalactic fields and are imaged in 19–45 photometric bands. In this work we use a subsample of galaxies with stellar mass $M_* > 10^{10}\ M_\odot$ in the redshift range $0.5 < z < 2.5$, corresponding to 12,235 galaxies.

2.2. Fitting Synthetic UVJ Fluxes

We also fit a grid of rest-frame *U*, *V*, and *J* fluxes to determine the constraining power of *UVJ* fluxes alone. These fluxes specify a single *UVJ* color and are given an arbitrary normalization. We generate 625 sets of *UVJ* fluxes corresponding to a regular grid in $0 < U\text{–}V < 2.5$ and $0 < V\text{–}J < 2.5$.

We fit these fluxes with the modified Prospector–α model described above. The mass–metallicity prior is replaced with a flat metallicity prior over $-1.0 < \log(Z/Z_\odot) < 0.2$ to ensure the analysis is independent of stellar mass. The maximum stellar age is set to 6 Gyr, corresponding to the age of the Universe at $z = 1$. The fluxes are assigned errors of 2.5%, though to preserve the *UVJ* colors the fluxes themselves are not perturbed.

3. Galaxy Properties in the *UVJ* Diagram

Williams et al. (2009) showed that *UVJ* selection can separate dusty star-forming galaxies from quiescent galaxies because dusty star-forming galaxies are red in *V*–*J* while quiescent galaxies are blue in *V*–*J*. While largely an empirical finding, this behavior was shown to be consistent with constrained dust models using fixed attenuation curves and parametric SFHs. However, there is a growing body of evidence suggesting that galaxies have a diversity of dust attenuation curves (Salmon et al. 2016; Leja et al. 2017; Narayanan et al. 2018; Salim et al. 2018) and a diversity of star formation histories (Pacifici et al. 2016; Iyer et al. 2019). Here, we use a more complex two-component dust model that allows variation in the shape of the dust attenuation curve and a flexible nonparametric distribution of stellar ages, allowing us to test the robustness of these conclusions to these assumptions.

Figure 1 shows how the SFH and dust posteriors change as a function of rest-frame *UVJ* colors.[1] The posteriors are derived by fitting the synthetic *UVJ* fluxes described in Section 2.2. This illustrates that *UVJ* colors continue to put robust constraints on both sSFR and dust attenuation even after allowing for the presence of confounding effects like age, stellar metallicity, and flexible dust models.

Figure 2 explores further trends between galaxy properties and *UVJ* colors. Galaxy properties are inferred both from synthetic *UVJ* fluxes and from fits to the observed UV–MIR SEDs. For the observed galaxies where many objects fall within a single *UVJ* pixel, the median value is shown. Only pixels containing at least 10 galaxies are shown. The maps are smoothed with a Gaussian with $\sigma = 1$ pixel in order to highlight trends.

Some of these parameters, such as M/L_g and dust attenuation, show strong and consistent trends whether fitting simple *UVJ* fluxes or the full photometric SED. These parameters are well constrained by *UVJ* colors alone. Other parameters, such as mean stellar age and metallicity, show no structure in *UVJ* space until they are constrained by the full photometric SED. These properties are either weakly constrained or not constrained by *UVJ* colors alone. This suggests that trends in the observed galaxies are induced by galaxy scaling relationships.

sSFR is a special case in this comparison. While the median sSFR of star-forming galaxies is unchanged when constrained with *UVJ* fluxes or the full SED, the median sSFR of quiescent galaxies becomes much lower. This is because galaxies with moderate sSFRs, e.g., sSFR $\sim 10^{-10.5}$ yr^{-1}, can also fall into the *UVJ*-quiescent region. This is a key result of this Letter and is discussed further in Section 4.

One important caveat is that it is not clear from the parameter maps alone whether these trends are being driven by the data or by assumptions built into the model. One way to distinguish between the two is to measure the difference between the prior and the posterior distributions. A reliable metric for this is the Kullback–Leibler divergence (hereafter $D_{\rm KL}$), defined as

$$D_{\rm KL} = \int_{-\infty}^{\infty} a(x) \ln\left(\frac{a(x)}{b(x)}\right) dx \quad (1)$$

for two probability distributions $a(x)$ and $b(x)$.

In Bayesian analysis, $D_{\rm KL}$ calculated from the prior $a(x)$ to the posterior $b(x)$ is interpreted as the information gained by fitting the data. If no information is gained, the prior and the posterior are identical and $D_{\rm KL} = 0$. As $D_{\rm KL}$ increases, the posterior and the prior become increasingly divergent.

Figure 3 is constructed in an analogous fashion to Figure 2 and shows $D_{\rm KL}$ from the prior to the posterior. The median $D_{\rm KL}$ for the galaxies in the pixel is shown for the full SED fits. The $D_{\rm KL}$ maps for the synthetic *UVJ* fluxes confirm our previous conclusions: M/L_g, dust attenuation, and the sSFR of star-forming galaxies are fairly well constrained by *UVJ* fluxes alone, while ages, metallicities, and the sSFRs of galaxies in the quiescent box are relatively unconstrained.

The average $D_{\rm KL}$ increases substantially when fitting the full photometric SED. This is expected, as the full SED provides more information than *UVJ* fluxes alone. However this provides necessary confirmation that UV–MIR photometry

[1] Here we adopt the *UVJ*-0quiescent selection criteria from Whitaker et al. (2012).

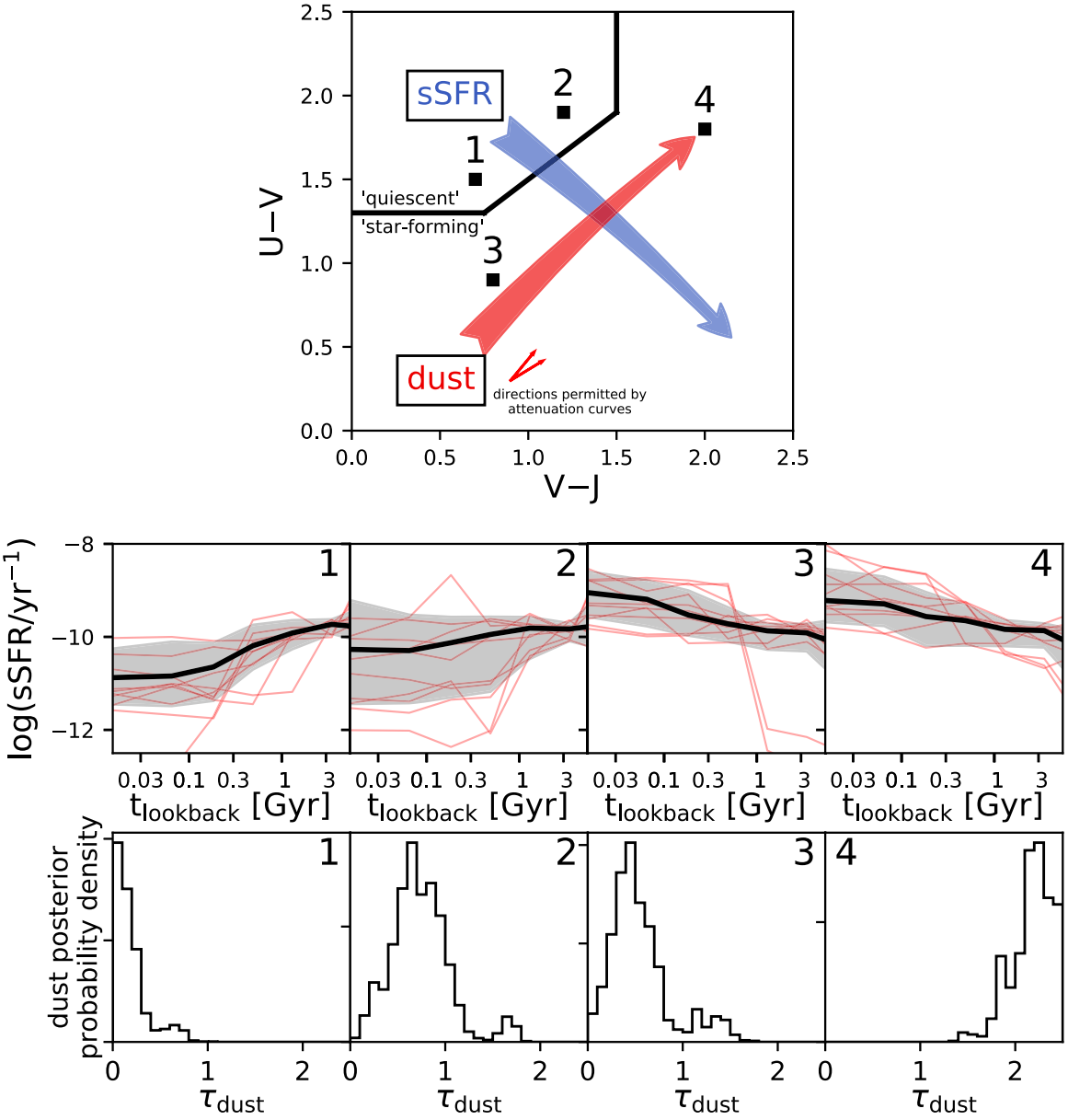

Figure 1. The top panel shows the *UVJ* diagram. The blue and red arrows show the effect of increasing sSFR and dust attenuation, respectively. The black arrows show the range of dust vector angles permitted by changes in the attenuation curve. The lines indicate the *UVJ*-quiescent selection box. The middle and lower panels show SFH and dust posteriors from fits to synthetic *UVJ* fluxes corresponding to the numbers in the top panel. For the SFHs, the black line is the posterior median, the gray shaded region is the 1σ posterior, and the thin red lines are random draws from the posterior. There is a clear mapping from *UVJ* colors to dust attenuation and the sSFRs of star-forming galaxies, but the quiescent region permits a wide range of recent sSFRs.

can put meaningful constraints on these parameters and implies that the trends observed in Figure 2 are reliable—though fitting spectroscopic data has the potential to provide much more precise measurements (e.g., Belli et al. 2019).

Taken together these results imply that the age and metallicity trends in the *UVJ* diagram are not specified by *UVJ* colors alone. Instead, galaxies must exist on some constrained plane in a high-dimensional parameter space (i.e., are subject to galaxy scaling relationships), with the shape of this plane then inducing correlations with *UVJ* colors. This means that these relationships can evolve with cosmological time. Indeed this evolution can be seen directly in the data: for example, the age-color trend in the quiescent box in Figure 2 is a combination of a mild age gradient at fixed redshift and the net evolution of the *UVJ* colors of the galaxy population across redshifts. Also, galaxies with sub-solar metallicity take about 3 Gyr to age into the *UVJ*-quiescent region (Tacchella et al. 2018), implying that *UVJ* selection will fail to identify low-metallicity quiescent galaxies at $z \gtrsim 3$.

We note that D_{KL} is not invariant to the chosen model. For example, the *UVJ*-quiescent region has a low D_{KL} for sSFR when constrained only by *UVJ* colors. This is partly because *UVJ* colors are not correlated with sSFR for sSFR $< 10^{-10.5}$ yr^{-1}, but also partly because the model is able to produce star-forming galaxies (sSFR $> 10^{-9}$ yr^{-1}) with *UVJ*-quiescent colors by combining significant dust attenuation with steep, SMC-like attenuation curves. Such galaxies likely do not exist in the real Universe due to the physical correlation between increasingly flat attenuation curves and increasing dust attenuation (e.g., Chevallard et al. 2013): however, they are

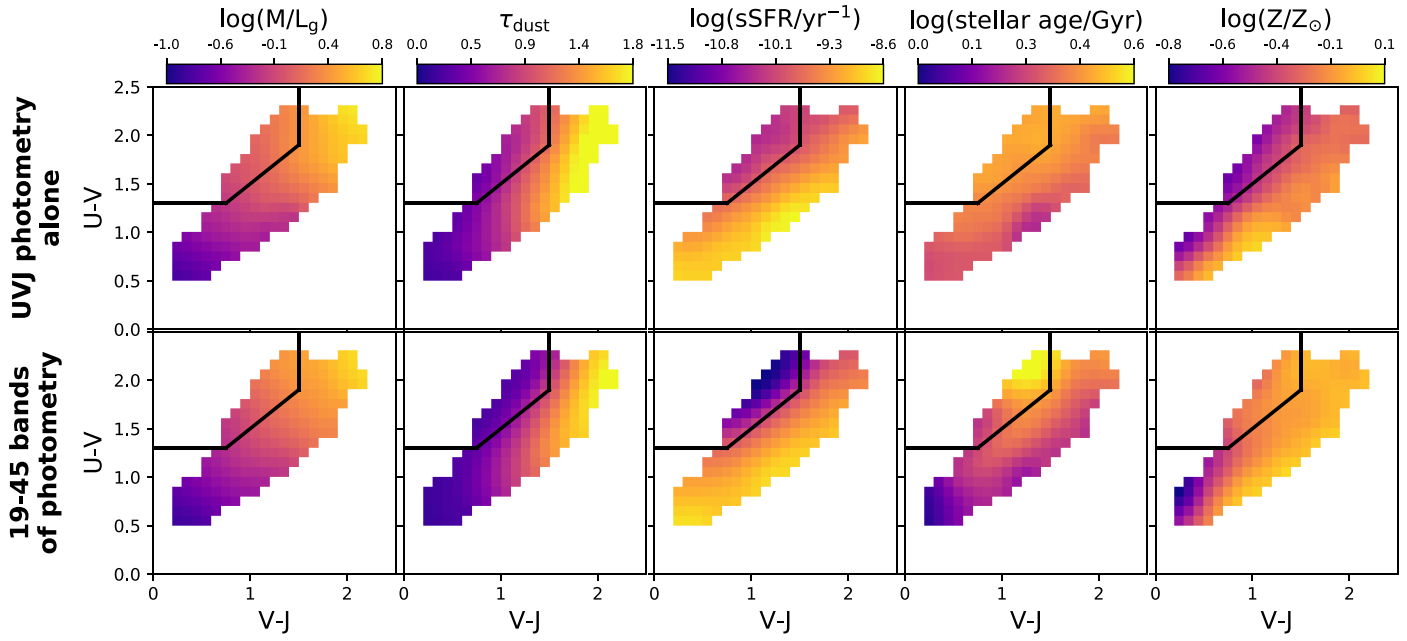

Figure 2. Median stellar population properties in the *UVJ* diagram after fitting synthetic *UVJ* fluxes (upper panels) and after fitting full SEDs of observed galaxies (lower panels). From right to left: mass-to-light ratio for the SDSS-*g* band relative to solar, dust optical depth, sSFR averaged over the most recent 100 Myr, average stellar age, and stellar metallicity. Each pixel shows either the median of the posterior (top rows) or the median parameter for galaxies in the *UVJ* pixel (bottom rows). Constraints from synthetic *UVJ* fluxes produce strong trends in dust and M/L_g and weak trends in sSFR, metallicity, and age. Comparatively, observed galaxies show stronger trends in sSFR and age and slightly stronger trends in metallicity. This difference implies that galaxies occupy a lower-dimensional parameter space than is permitted by their *UVJ* colors alone.

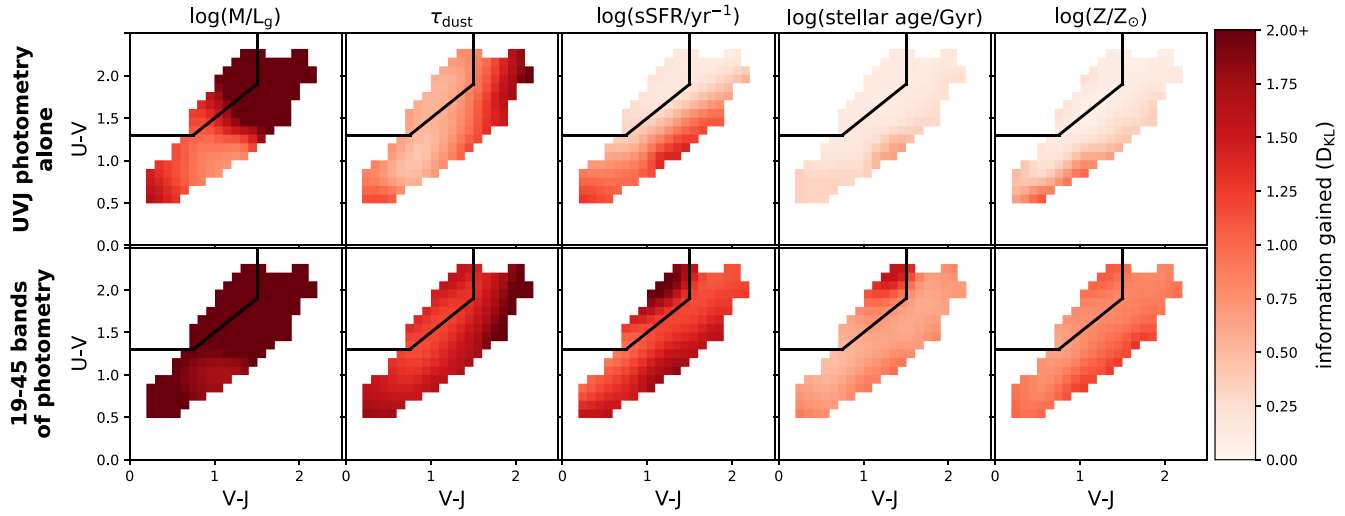

Figure 3. Information gained after fitting synthetic *UVJ* fluxes (upper panels) and full observed SEDs (lower panels). The overall layout of the figure follows Figure 2. We quantify the information gained from the data by calculating the Kullback–Leibler divergence ($D_{\rm KL}$) between the prior and the posterior. We find that synthetic *UVJ* fluxes put tight constraints on $M/L_{\rm g}$ and dust attenuation, partial constraints on sSFR, and minimal constraints on metallicity and age. The lower panels demonstrate that full SED fits put more meaningful constraints on these parameters, confirming that the trends in the bottom panels of Figure 2 are data-driven rather than a consequence of model assumptions.

not ruled out a priori by the model, resulting in a lower-than-expected $D_{\rm KL}$. The full SED fits are robust to this effect as the full SED can reliably rule out the combination of high dust attenuation and steep attenuation curves.

4. Beyond *UVJ*

The fact that quiescent *UVJ* colors from the quiescent region do not appear to specify low sSFRs merits further investigation. While the *UVJ* diagram was designed to distinguish between star-forming and quiescent galaxies, Figures 2 and 3 together suggest that the *UVJ*-quiescent selection cannot distinguish between moderate and low sSFRs. This is consistent with observational findings that ∼10%–30% of *UVJ*-quiescent galaxies host significant ongoing star formation (Belli et al. 2017; Díaz-García et al. 2017; Schreiber et al. 2018).

Figure 4 examines the correlation between rest-frame colors and quiescence directly by plotting the relationship between several rest-frame colors and $\log(\mathrm{sSFR}/\mathrm{yr}^{-1})$ inferred from the `Prospector` fits to the 3D-*HST* photometry. The sSFR direction in *UVJ* space is defined as the perpendicular direction

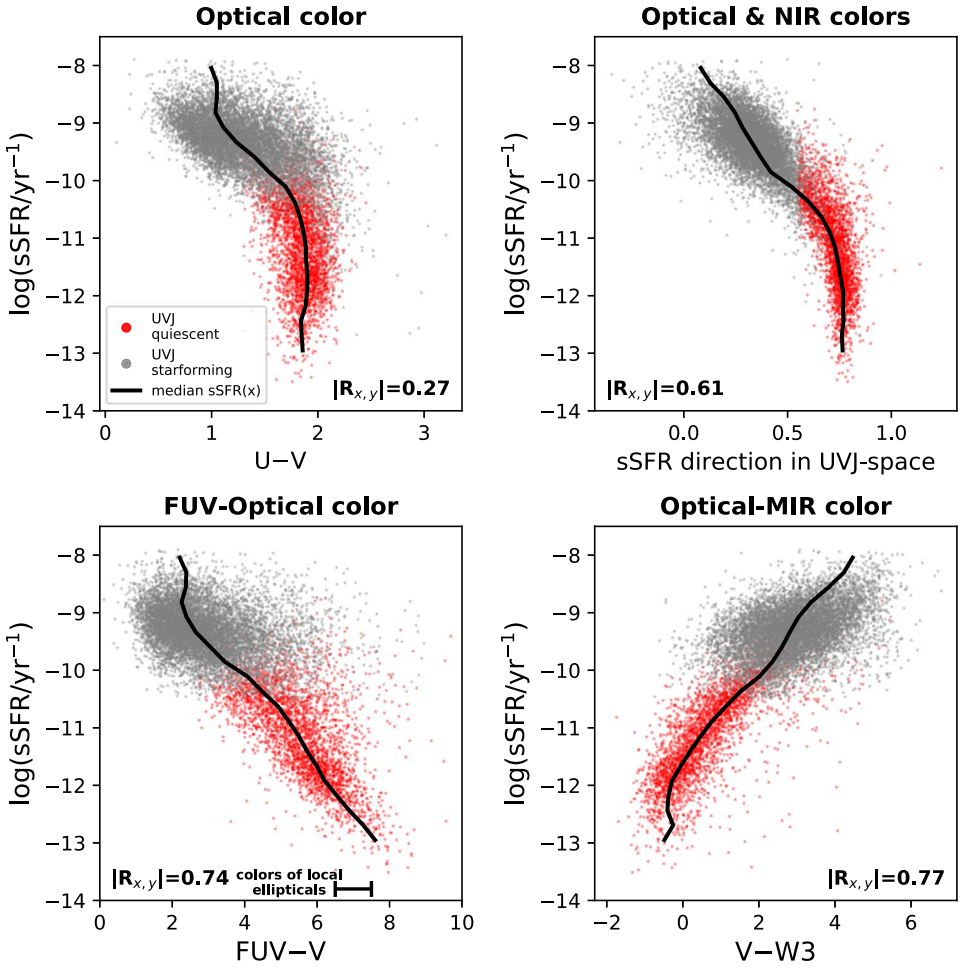

Figure 4. The correlation between sSFR and optical color, *UVJ* colors, UV–optical color, and optical–MIR color is shown. The Pearson correlation coefficient between color and sSFR is shown in the corner. Optical and NIR colors begin to saturate at approximately sSFR $\sim 10^{-10.5}$ yr^{-1}, whereas FUV–optical or optical–MIR colors continue to correlate with sSFR over a wide range of values. The median sSFR as a function of color is shown as a black line. The approximate range of colors for local elliptical galaxies is shown as a black bar in the FUV–*V* diagram (Jeong et al. 2009), as described in the text.

to the quiescent selection line (Fang et al. 2018), indicated by the blue arrow in Figure 1.

This figure demonstrates the well-known fact that *U*–*V* colors alone cannot distinguish between star-forming and quiescent galaxies (e.g., Eales et al. 2017). It further shows that while *UVJ* colors partially break this degeneracy, the correlation between color and sSFR begins to saturate at sSFR $< 10^{-10.5}$ yr^{-1} and is fully saturated by sSFR $= 10^{-11}$ yr^{-1}.

The lower panels show how this relationship can be restored by instead using colors calculated with far-UV (FUV) or mid-infrared (MIR) fluxes, i.e., *GALEX* FUV ($\lambda_{\rm rest} \sim 1500$ Å) and *WISE* W3 ($\lambda_{\rm rest} \sim 12$ μm). Colors constructed with these fluxes correlate with sSFR down to low sSFRs. The correlation between rest-frame color and sSFR is calculated using the Pearson correlation coefficient, shown in the corner of each panel. The increasing coefficient suggests that quiescent galaxies can be more cleanly identified with FUV or MIR fluxes. We note that the outliers in the *V*–W3–sSFR relationship are almost entirely galaxies with significant mid-IR AGN emission: removing such galaxies using AGN indicators such as X-ray luminosities will further increase the efficacy of this selection.

One concern is that hot evolved stars can produce very blue colors that masquerade as star formation in the FUV (e.g., Han et al. 2007). We include observed FUV–*V* colors from local quiescent galaxies as a rough upper bound for the size of this effect (Jeong et al. 2009). Notably, the abundance of hot evolved stars is difficult to predict even in local star clusters and may evolve significantly with redshift (e.g., Conroy & Gunn 2010).

In Figure 5, we plot 3D-*HST* galaxies color-coded by sSFR to contrast the performance of the *UVJ* diagram with FUV/MIR color–color diagrams. We optimize the dividing line in color–color space to maximize the "purity" of both quiescent and star-forming populations as sorted by their posterior median colors. Purity is defined as the fraction of galaxies in the quiescent (star-forming) box whose `Prospector`-inferred sSFRs are below (above) the target sSFR. This is done for a range of target sSFRs, and sample purity as a function of sSFR is shown below each color–color diagram. We simulate the effect of measurement uncertainty by drawing from the color posterior many times. The resulting median purities of the color–color selection are shown as dashed lines.

All of the diagrams perform fairly well at sSFR$_{\rm cut} \sim 10^{-10}$ yr^{-1}. However, for lower sSFRs the *UVJ* diagram becomes increasingly inefficient, while the FUV+MIR color–color diagram remains near 100% purity even after accounting for the effects of measurement uncertainty. This suggests that

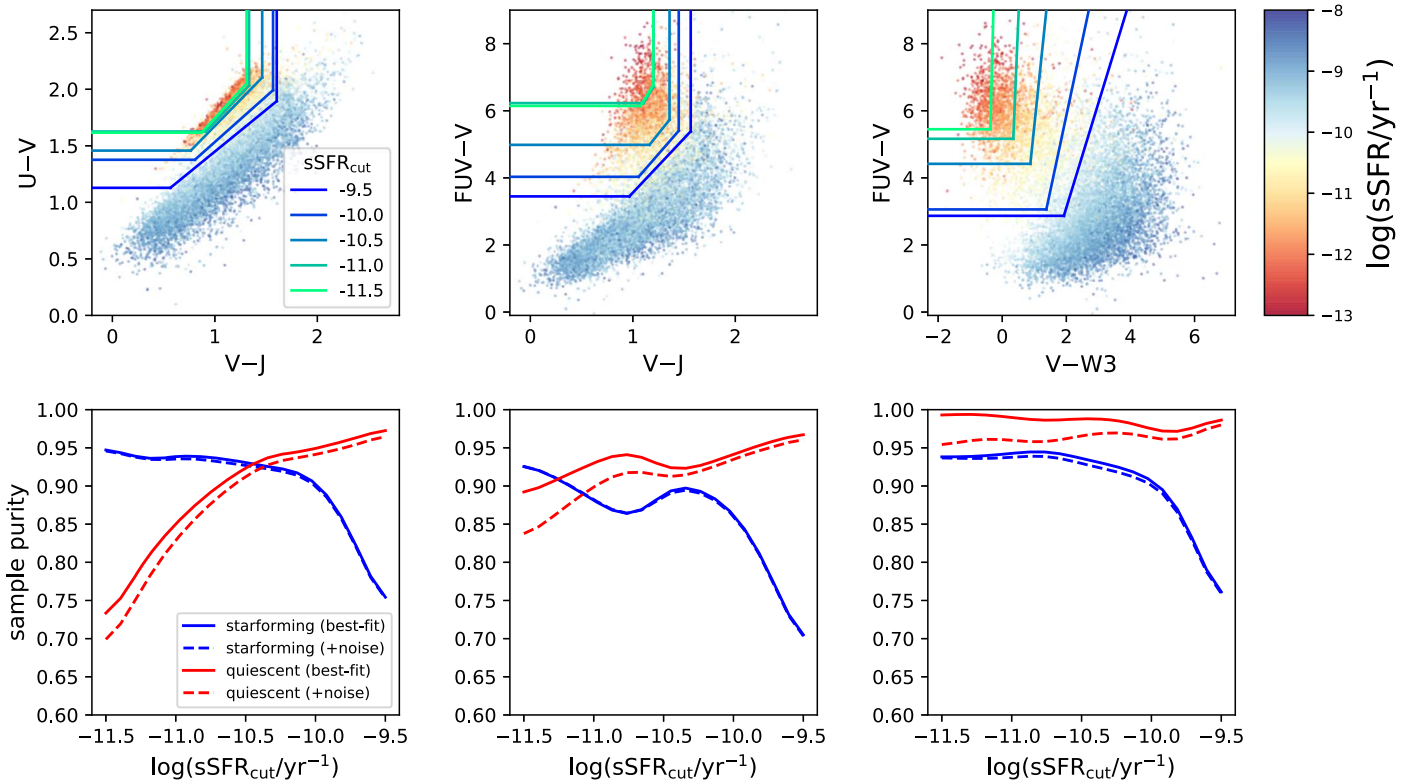

Figure 5. Comparison of the efficiency of sample selection by galaxy sSFR in different color–color spaces. In the upper row, from left to right, the panels show the canonical *UVJ* diagram, the FUV–*V*–*J* diagram, and the FUV–*V*–W3 diagram. In the lower row, the sample purity as a function of target sSFR is shown, both for the best-fitting colors (solid line), and for modeling the effect of photometric uncertainty (dashed lines). All of the color–color diagrams perform well at $\mathrm{sSFR_{cut}} \sim 10^{-10}$ yr^{-1}, but for lower sSFRs the *UVJ* diagram becomes increasingly inefficient while the FUV/MIR color–color diagrams remain near 100% purity.

FUV/MIR fluxes are a more efficient method to select galaxies with low or very low sSFRs.

Here we report the best-fit color–color divisions for $\log(\mathrm{sSFR_{cut}}/\mathrm{yr}^{-1}) = (-9.5,\ -10.5,\ -11.5)$, respectively. Galaxies are defined as quiescent when their rest-frame colors meet the following criteria:

$$y > ax + b, \tag{2}$$

$$x > c, \tag{3}$$

$$y > d. \tag{4}$$

For the *V*–*J*, *U*–*V* diagram, $a = (0.74, 0.93, 0.99)$, $b = (0.71, 0.75, 0.75)$, $c = (1.13, 1.46, 1.62)$, and $d = (1.6, 1.46, 1.31)$.

For the *V*–*J*, FUV–*V* diagram, $a = (3.24, 3.84, 5.03)$, $b = (0.32, 0.52, 0.74)$, $c = (3.45, 4.98, 6.14)$, and $d = (1.56, 1.36, 1.20)$.

For the *V*–*W*3, FUV–*V* diagram, $a = (3.12, 9.17, 37.73)$, $b = (-3.13, -3.62, 19.40)$, $c = (2.87, 4.42, 5.45)$, and $d = (119.07, 63.82, 11.79)$.

5. Summary and Discussion

Here we have used Bayesian inference to show that many galaxy properties are well-correlated with their rest-frame *UVJ* colors. By comparing these observed correlations to fits to synthetic *UVJ* fluxes, we have demonstrated that correlations with M/L_g, dust attenuation, and sSFR are caused by a unique mapping from colors to galaxy properties, whereas correlations with stellar age and stellar metallicity are most likely driven by galaxy scaling relationships. We have used the Kullback–Leibler divergence to show that these correlations are not driven by our model priors. We have further demonstrated that the relationship between *UVJ* colors and sSFR begins to saturate at $\log(\mathrm{sSFR}/\mathrm{yr}^{-1}) \sim -10.5$, effectively meaning there is no sSFR–color relationship below this limit. Finally, we show that the sSFR–color relationship remains robust to low levels when instead using color–color selection with FUV/MIR fluxes, and we present selection criteria in these new spaces.

First, our findings reaffirm the well-established fact that *UVJ* selection is largely successful in dividing the galaxy population into star-forming and quiescent systems (Fumagalli et al. 2014). The key niche filled by the proposed new color–color diagrams is their sensitivity to sSFR below $\mathrm{sSFR} \sim 10^{-10.5}$ yr^{-1}, permitting the selection of a pure sample of low-sSFR galaxies. Sample selection often involves choosing tradeoffs between purity and completeness, and optimizing for completeness produces different selection criteria that are appropriate for different science goals. A more pure quiescent sample likely will increase the efficiency of searches for high-redshift quiescent galaxies (e.g., Schreiber et al. 2018), and may also produce cleaner distinctions between the structure of quiescent and star-forming galaxies (e.g., Hill et al. 2019).

One challenge is that FUV and mid-IR photometry is not always readily available. The rest-frame FUV is easily accessible for high-redshift galaxies, as it corresponds to the observed-frame UV/optical. At lower redshifts ($z \lesssim 0.5$) the FUV is only accessible through *GALEX*, which has lower sensitivity and angular resolution. The most robust color–color diagram requires MIR detections or upper limits. While such data are currently difficult to obtain, the upcoming launch of *JWST* will allow observations of the rest-frame MIR out to $z \sim 1$.

This is not the first work that proposes color selection extending farther into the UV. Multiple studies find that *GALEX* NUV–*r* is an excellent indicator of current versus past star formation activity (Martin et al. 2007) and Arnouts et al. (2007, 2013). Ilbert et al. (2013) note many of the same advantages in NUV–*r* that are found here in FUV–*V*, such as a better dynamic range than *U*–*V* and easier access in high-redshift galaxies. We note that tests in our framework have shown that *FUV*-based colors have a somewhat stronger correlation with sSFR than NUV-based colors.

These results also suggest that *UVJ* classification should be applied with care to spatially resolved photometry (e.g., Liu et al. 2017). It remains to be seen whether *UVJ* trends that are significantly affected by galaxy scaling relationships also hold on spatially resolved scales.

Finally we note that, while color–color diagrams are a straightforward and economic choice for sample selection, more precise and accurate statements about galaxy properties can often be made by fitting models to the observed SED.

We thank Benjamin Johnson, Pieter van Dokkum, and Marijn Franx for thoughtful discussions. J.L. is supported by an NSF Astronomy and Astrophysics Postdoctoral Fellowship under award AST-1701487. S.T. is supported by the Smithsonian Astrophysical Observatory through the CfA Fellowship. The computations in this paper were run on the Odyssey cluster supported by the FAS Division of Science, Research Computing Group at Harvard University.

ORCID iDs

Joel Leja https://orcid.org/0000-0001-6755-1315
Sandro Tacchella https://orcid.org/0000-0002-8224-4505
Charlie Conroy https://orcid.org/0000-0002-1590-8551

References

Arnouts, S., Le Floc'h, E., Chevallard, J., et al. 2013, A&A, 558, A67
Arnouts, S., Walcher, C. J., Le Fèvre, O., et al. 2007, A&A, 476, 137
Baldry, I. K., Glazebrook, K., Brinkmann, J., et al. 2004, ApJ, 600, 681
Balogh, M. L., Baldry, I. K., Nichol, R., et al. 2004, ApJL, 615, L101
Barro, G., Faber, S. M., Pérez-González, P. G., et al. 2014, ApJ, 791, 52
Belli, S., Genzel, R., Förster Schreiber, N. M., et al. 2017, ApJL, 841, L6
Belli, S., Newman, A. B., & Ellis, R. S. 2019, ApJ, 874, 17
Brinchmann, J., Charlot, S., White, S. D. M., et al. 2004, MNRAS, 351, 1151
Chabrier, G. 2003, PASP, 115, 763
Charlot, S., & Fall, S. M. 2000, ApJ, 539, 718
Chevallard, J., Charlot, S., Wandelt, B., & Wild, V. 2013, MNRAS, 432, 2061
Conroy, C., & Gunn, J. E. 2010, ApJ, 712, 833
Conroy, C., Gunn, J. E., & White, M. 2009, ApJ, 699, 486
Daddi, E., Cimatti, A., Renzini, A., et al. 2004, ApJ, 617, 746
Davé, R., Rafieferantsoa, M. H., & Thompson, R. J. 2017, MNRAS, 471, 1671
Díaz-García, L. A., Cenarro, A. J., López-Sanjuan, C., et al. 2017, arXiv:1711.10590
Donnari, M., Pillepich, A., Nelson, D., et al. 2019, MNRAS, 485, 4817
Eales, S., de Vis, P., Smith, M. W. L., et al. 2017, MNRAS, 465, 3125
Fang, J. J., Faber, S. M., Koo, D. C., et al. 2018, ApJ, 858, 100
Fumagalli, M., Labbé, I., Patel, S. G., et al. 2014, ApJ, 796, 35
Han, Z., Podsiadlowski, P., & Lynas-Gray, A. E. 2007, MNRAS, 380, 1098
Hill, A. R., van der Wel, A., Franx, M., et al. 2019, ApJ, 871, 76
Hinshaw, G., Larson, D., Komatsu, E., et al. 2013, ApJS, 208, 19
Ilbert, O., McCracken, H. J., Le Fèvre, O., et al. 2013, A&A, 556, A55
Iyer, K. G., Gawiser, E., Faber, S. M., et al. 2019, ApJ, 879, 116
Jeong, H., Yi, S. K., Bureau, M., et al. 2009, MNRAS, 398, 2028
Johnson, B., & Leja, J. 2017, bd-j/prospector: Initial release, version 0.3, Zenodo, doi:10.5281/zenodo.1116491
Kauffmann, G., Heckman, T. M., White, S. D. M., et al. 2003, MNRAS, 341, 33
Leja, J., Carnall, A. C., Johnson, B. D., Conroy, C., & Speagle, J. S. 2019a, ApJ, 876, 3
Leja, J., Johnson, B. D., Conroy, C., et al. 2019b, ApJ, 877, 140
Leja, J., Johnson, B. D., Conroy, C., & van Dokkum, P. 2018, ApJ, 854, 62
Leja, J., Johnson, B. D., Conroy, C., van Dokkum, P. G., & Byler, N. 2017, ApJ, 837, 170
Liu, F. S., Jiang, D., Faber, S. M., et al. 2017, ApJL, 844, L2
Martin, D. C., Wyder, T. K., Schiminovich, D., et al. 2007, ApJS, 173, 342
Merlin, E., Fontana, A., Castellano, M., et al. 2018, MNRAS, 473, 2098
Moresco, M., Pozzetti, L., Cimatti, A., et al. 2013, A&A, 558, A61
Narayanan, D., Davé, R., Johnson, B. D., et al. 2018, MNRAS, 474, 1718
Pacifici, C., Kassin, S. A., Weiner, B. J., et al. 2016, ApJ, 832, 79
Papovich, C., Kawinwanichakij, L., Quadri, R. F., et al. 2018, ApJ, 854, 30
Salim, S., Boquien, M., & Lee, J. C. 2018, ApJ, 859, 11
Salmon, B., Papovich, C., Long, J., et al. 2016, ApJ, 827, 20
Schreiber, C., Glazebrook, K., Nanayakkara, T., et al. 2018, A&A, 618, A85
Skelton, R. E., Whitaker, K. E., Momcheva, I. G., et al. 2014, ApJS, 214, 24
Speagle, J. S. 2019, arXiv:1904.02180
Straatman, C. M. S., Labbé, I., Spitler, L. R., et al. 2014, ApJL, 783, L14
Strateva, I., Ivezić, Ž., Knapp, G. R., et al. 2001, AJ, 122, 1861
Tacchella, S., Bose, S., Conroy, C., Eisenstein, D. J., & Johnson, B. D. 2018, ApJ, 868, 92
Whitaker, K. E., Kriek, M., van Dokkum, P. G., et al. 2012, ApJ, 745, 179
Whitaker, K. E., van Dokkum, P. G., Brammer, G., et al. 2013, ApJL, 770, L39
Williams, R. J., Quadri, R. F., Franx, M., van Dokkum, P., & Labbé, I. 2009, ApJ, 691, 1879
Wuyts, S., Labbé, I., Franx, M., et al. 2007, ApJ, 655, 51